

Efficient, simulation-free estimators of firing rates with Markovian surrogates

Zhongyi Wang and Aaditya Rangan

Courant Institute of Mathematical Sciences, New York University, New York, NY, 10003, USA

Louis Tao*

*Center for Bioinformatics, National Laboratory of Protein Engineering and Plant Genetic Engineering,
School of Life Sciences, Peking University, Beijing, 100871, China; and*

Center for Quantitative Biology, Academy for Advanced Interdisciplinary Studies, Peking University, Beijing, 100871, China

Zhuo-Cheng Xiao†

NYU-ECNU Institute of Brain and Cognitive Science, and

NYU-ECNU Institute of Mathematical Sciences, New York University Shanghai, Shanghai, 200124, China

(Dated: May 14, 2025)

Spiking neural networks (SNNs) are powerful mathematical models to integrate the biological details of neural systems, but their complexity often makes them computationally expensive and analytically untractable. The firing rate of an SNN is a crucial first-order statistic for characterizing network activity. However, estimating firing rates analytically from even simplified SNN models is challenging due to 1) the intricate dependence between the nonlinear network dynamics and parameters, and 2) the singularity and irreversibility of spikes. In this Letter, we propose a class of computationally efficient, simulation-free estimators of firing rates. This is based on a hierarchy of Markovian approximations that reduces the complexity of SNN dynamics. We show that while considering firing rates alone is insufficient for accurate estimation of themselves, the information of spiking synchrony dramatically improves the estimator's accuracy. This approach provides a practical tool for brain modelers, directly mapping biological parameters to firing rate.

I. INTRODUCTION

Spiking neural networks (SNNs) provide a powerful framework for modeling neural dynamics and are widely used in computational neuroscience [1–12]. A key challenge in studying SNNs is extracting meaningful dynamical features that reveal how physiological mechanisms give rise to emergent brain functions [13–15]. However, both analytical approaches and direct simulations face significant obstacles. The discrete, high-dimensional nature of SNNs makes mathematical analysis intractable, while large-scale simulations become computationally prohibitive as network size increases [16–19]. In practice, both theoretical and experimental neuroscientists are often primarily interested in long-term statistical properties of SNN dynamics, such as neuronal firing rates, which serve as fundamental indicators of neural activity [20–23]. Thus, there is a pressing need for efficient analytical methods that can approximate these steady-state statistics without resorting to extensive simulations.

In this Letter, we introduce a Markovian approximation that systematically maps SNN dynamics onto state transitions while preserving essential statistical properties. By treating neuron states as discrete random variables, our approach allows for the derivation of a hierarchy of analytically tractable approximations, enabling direct computation of long-term dynamic statistics via the invariant measure of the reduced model.

We propose two simulation-free estimators of firing rates. The first estimator prioritizes computational efficiency but does not account for temporal synchrony, while the second explicitly captures the temporal correlations of synaptic inputs, leading to greater predictive accuracy in networks with varying degrees of synchronicity. To our knowledge, the second estimator is the first simulation-free computational tool for finite-size SNNs that is not constrained by specific parameter choices or dynamic regimes [24, 25]. Compared to previous theoretical approaches, such as mean-field theories and Fokker-Planck equations, our method reduces estimation errors by magnitudes. This is done by incorporating higher-order statistical features—specifically, the degree of spiking synchrony reflected in synaptic inputs—demonstrating the importance of synchrony in shaping network dynamics.

II. LEAKY INTEGRATE-AND-FIRE NETWORKS

In this Letter, we demonstrate an efficient firing-rate estimator for leaky integrate-and-fire (LIF) networks. LIF networks are widely used in computational neuroscience to model brain circuits [1–12, 15, 26]. Here, we focus on a network of N -neuron LIF networks consisting of two neuronal populations: N^E excitatory (E) and N^I inhibitory (I) cells ($N = N^E + N^I$). This setup is commonly used to study the dynamics of local brain circuits [27–31].

Consider a LIF neuron i of type $X \in \{E, I\}$, the dy-

* taolt@mail.cbi.pku.edu.cn

† xiao.zc@nyu.edu

namics of its membrane potential $V_i(t)$ are governed by

$$\frac{dV_i}{dt} = g_i^{X,\text{leak}}(V^{\text{rest}} - V_i) + g_i^E \cdot (V^E - V_i) + g_i^I \cdot (V^I - V_i) + I_i^{\text{ext}}, \quad (1)$$

where $g_i^{X,\text{leak}}$ represents the leakage conductance, V^{rest} is the resting potential, V^E and V^I are the reversal potentials for excitatory and inhibitory currents, respectively. When V_i reaches a threshold potential $V^{X,\text{th}}$, the neuron i instantly releases a type- X spike which is sent to its post-synaptic neurons, then V_i enters a refractory state \mathcal{R} for a period of τ^{ref} before reset to V^{rest} . During the refractory period, the neuron remains unresponsive to incoming stimuli.

The synaptic conductances (g_i^E, g_i^I) and the external input current I_i^{ext} are given by

$$g_i^Y(t) = \sum_{j \in Y, j \neq i} S_{ij} \sum_{\mu_j^Y} G^Y(t - t_{\mu_j^Y}), \quad Y = E, I, \quad (2)$$

$$I_i^{\text{ext}}(t) = S_i^{\text{ext}} \sum_{\mu_i^{\text{ext}}} G^{\text{ext}}(t - t_{\mu_i^{\text{ext}}}), \quad (3)$$

Here, S_{ij} stands for the synaptic coupling strength from neuron j to i , and S_i^{ext} denotes the input synaptic coupling strength to neuron i ; $t_{\mu_j^Y}$ are the spiking times of neuron j , and $t_{\mu_i^{\text{ext}}}$ are spiking times of the input; $G^X(t), X \in \{\text{ext}, E, I\}$ is the synaptic kernel for type- X neurons or the input synaptic kernel, given by

$$G^X(t) = \frac{1}{\tau^X} \exp\left(-\frac{t}{\tau^X}\right) \cdot H(t),$$

where τ^X is the timescale of type- X synaptic dynamics, and $H(t)$ is the Heaviside function.

We note that, a fundamental source of complexity in spiking neural network (SNN) dynamics is the singular impact of spikes on postsynaptic neurons, combined with the irreversible nature of the spike-generation process in presynaptic neurons. This fire-refractory-reset mechanism is a defining feature of most SNN models and is essential for capturing the physiological details of spiking communication in the brain.

III. A MARKOVIAN APPROXIMATION

Our previous study introduced a Markovian approximation of the LIF network and a subsequent coarse-grained reduction. This section provides a concise review of that framework and outlines two computationally efficient firing-rate estimators derived from it.

To treat the membrane potential $V_i(t)$ as a Markov chain, we discretize the interval $(V^I, V^{X,\text{th}}) \cup \mathcal{R}$ appropriately and determine the discrete analogs of each term in Eq. (1). The discretized membrane potential of a type- X neuron i takes values in the state space

$$\Gamma := \{-m^I, -m^I + 1, \dots, -1, 0, 1, \dots, m^{X,\text{th}} - 1\} \cup \{\mathcal{R}\},$$

where $-m^I$ and $m^{X,\text{th}}$ correspond to V^I and $V^{X,\text{th}}$, respectively. A state $m \in \Gamma$ corresponds to potentials $V_i \in [ma, (m+1)a]$, where the voltage bin size is $a = \frac{V^{X,\text{th}} - V^I}{m^{X,\text{th}} - m^I}$.

To handle the singular nature of synaptic inputs as presynaptic spikes, whose temporal effects are modeled by the synaptic kernel $G^X(t)$, we introduce discrete variables $H_i^Y \in \mathbb{N}$, $Y \in \{\text{ext}, E, I\}$, replacing the continuous conductances g_i^Y in Eq. (1). These variables, termed "pending kick pools," accumulate discrete synaptic kicks whenever neuron i receives presynaptic spikes. Each pending kick induces a state transition and is removed after an exponentially distributed waiting time $\tau \sim \text{Exp}(\tau^Y)$, making H_i^Y a birth-death process.

Thus, the network's dynamic state is initially described by a $4N$ -dimensional tuple:

$$\omega = (v_1, \dots, v_N, H_1^E, \dots, H_N^E, H_1^I, \dots, H_N^I, H_1^{\text{ext}}, \dots, H_N^{\text{ext}}).$$

Since the external input timescale τ^{ext} is zero, we omit the last N terms, as external kicks do not accumulate.

The large dimensionality of this Markovian model demands further simplification for practical analysis. To achieve this, we coarse-grain the system by assuming rapid decorrelation of each neuron's synaptic drive H_i^X from its past (**Assumption 1**, see [32]). This assumption naturally follows from the annealed network structure. Consequently, any two neurons of the same type sharing the same membrane potential become statistically indistinguishable. The reduced Markovian dynamics are then described by population-level empirical distributions (ρ^E, ρ^I) and four synaptic drive variables $(H^{EE}, H^{EI}, H^{IE}, H^{II})$. Here,

$$\rho^X = \frac{1}{N^X} \cdot (n_{-m^I}^X, \dots, n_{m^{X,\text{th}}-1}^X, n_{\mathcal{R}}^X), \quad \sum_{m \in \Gamma} n_m^X = N^X.$$

Long-term averages of dynamical statistics such as network firing rates can be inferred from single-neuron statistics due to the network's homogeneity and ergodicity (see [33, 34]). Therefore, we focus on individual E - and I -neurons whose state transitions occur within one of five defined scenarios during an infinitesimal time step dt (see Appendix A). The transition rates depend explicitly on synaptic drives H^{QR} .

Given empirical distributions ρ_t^X and synaptic drives H_t^{XY} , we construct a transition rate matrix $Q_X = Q_X(H_t^{XE}, H_t^{XI})$, where $Q_X(i; j)$ denotes transition rates from state i to j , and $Q_X(i; i) = -\sum j \neq i Q_X(i; j)$. Consequently, the evolution of ρ_t^X follows the Kolmogorov forward equation:

$$\frac{d}{dt} \rho_t^X = \rho_t^X Q_X(H_t^{XE}, H_t^{XI}). \quad (4)$$

To close this system, we approximate synaptic drives by their expectations \bar{H}_t^{XY} , which follow birth-death dynamics:

$$\frac{d}{dt} \bar{H}_t^{XY} = -\frac{\bar{H}_t^{XY}}{\tau^{XY}} + N^Y P^{XY} f_t^Y, \quad (5)$$

where instantaneous firing rates f^E and f^I are computed from the membrane potential distribution ρ_t^X (see Appendix B).

Equations (4) and (5) fully describe the evolution of single-neuron statistics, from which long-term averages, such as firing rates, can be readily computed. From these equations, we propose two firing-rate estimators:

- **Type I:** Assumes homogeneous firing patterns (no temporal synchrony). The steady-state firing rates f^X are computed from:

$$0 = \rho_\infty^X Q_X(\bar{H}^{XE}, \bar{H}^{XI}), \quad (6)$$

$$0 = -\frac{\bar{H}^{XY}}{\tau^{XY}} + N^Y f^Y P^{XY}, \quad (7)$$

$$f^X = \frac{\rho_\infty^X(m^{X,\text{th}})}{\tau^{X,\text{ref}}}. \quad (8)$$

- **Type II:** Removes the homogeneity assumption and incorporates temporal synchrony through the dynamic evolution of H^{QR} from Eqs. (4) and (5). The long-term firing rate averages are obtained from any potential limit-cycle solutions.

We conclude this section with two key insights. First, although the simplest estimator (Type I) ignores temporal synchrony, our results demonstrate that even a minimal account of synchrony—such as in the Type II estimator—substantially improves the accuracy of firing rate predictions. Second, leveraging only first-order statistics, specifically the expectations of synaptic inputs, is already sufficient to achieve high accuracy in many regimes. This underscores the practical strength of the Type II estimator despite its simplicity. Nonetheless, future work exploring higher-order moment closures may further deepen our understanding of neuronal dynamics, especially in regimes where fluctuations in synchrony have functionally significant effects.

IV. RESULTS

This section presents numerical results for the two firing rate estimators—Type I and Type II—and compares their performance with previously proposed methods. We begin by demonstrating that the Type I estimator accurately reproduces single-neuron responses to external Poisson inputs, then show its limitations in highly synchronous network regimes. In contrast, the Type II estimator performs well in conditions where the Type I estimator fails, particularly when network synchrony depends sensitively on timescale parameters. Finally, we benchmark both estimators against two established mean-field-based approaches (MF+v [35] and the mean-driven limit [36, 37]). Our results highlight that our methods strike a favorable balance between predictive accuracy and computational efficiency, requiring less CPU time while maintaining or exceeding the accuracy of traditional approaches.

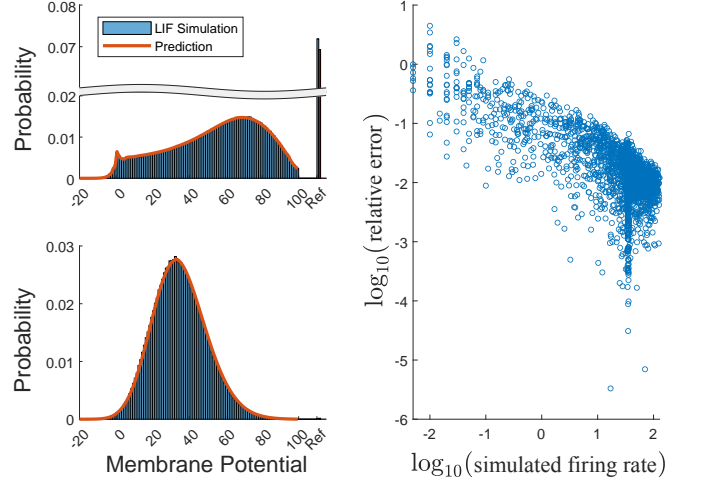


FIG. 1. Approximation of a single neuron which receives upstream Poisson inputs with constant rates. **Left:** detailed comparison of predicted steady-state voltage distribution and long-time average from simulation, with two sets of parameters; **Right:** relative predictive error versus long-time average firing rate from simulation on log-log scale, with 3000 sets of parameters, in which recurrent input rates, refractory periods and external input rates are varied.

Type I estimator for single neurons. We first evaluate the Type I estimator on single LIF neurons driven by Poissonian inputs (Fig. 1). This setting mimics a neuron embedded in a larger, asynchronous SNN, where recurrent inputs from E and I populations are statistically independent and temporally homogeneous. The constant Poisson input rates, f_{rec}^E and f_{rec}^I , allow us to remove Eq. (8), reducing the system to a linear problem. The remaining equations are then solved by computing the left null vector of the transition matrix Q_X , yielding the invariant voltage distribution ρ_∞^X , from which the steady-state firing rate is read via Eq. (8).

To validate this approach, we compare the predictions of the Type I estimator with ground truth data obtained from LIF simulations ($T = 100$ s, $\delta t = 0.1$ ms). We evaluate performance across 3000 parameter configurations, varying recurrent input rates (0–75 Hz), refractory periods (0.8–2.3 ms), and external input rates (100–10,000 Hz). Fig. 1A shows a representative case where the predicted ρ_∞^X aligns closely with simulation results. Fig. 1B summarizes the firing rate predictions across all test cases, with a maximum relative error of only 4.77%. Moreover, the estimator performs better at higher firing rates, as indicated by a clear negative trend in error on the log-log plot. Overall, the Type I estimator provides robust and accurate performance for single-neuron firing rate estimation under asynchronous input conditions.

Type I estimator for spiking networks. Encouraged by the single-neuron results, we next apply the Type I estimator to the fully recurrent SNNs described in Sect.II. Eqs.(6–8) are linear and can be solved by initializing a

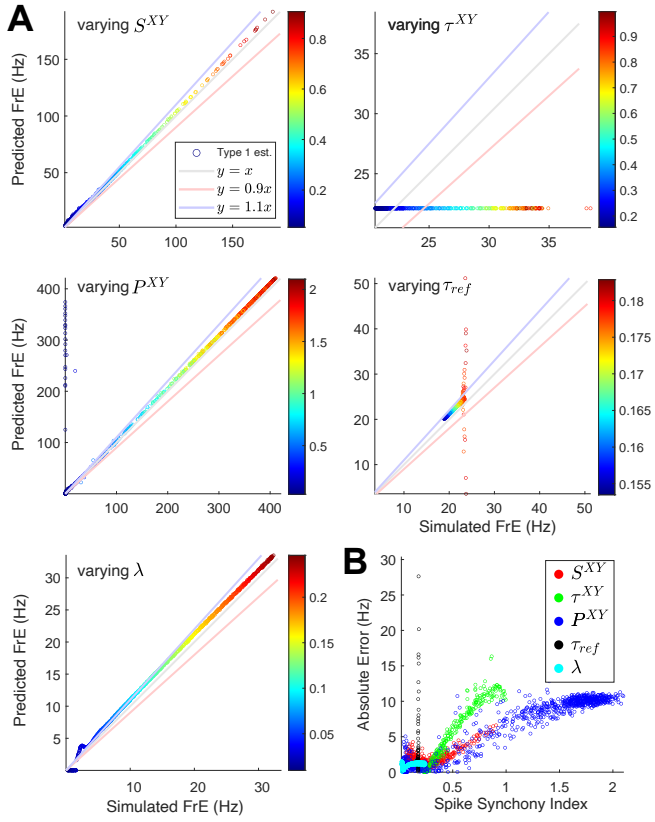


FIG. 2. Predictions of the simplified method versus ground truth from simulations. Colors of dots reflect the spike synchrony index of LIF simulations of SNN dynamics. **A:** comparison of predicted steady-state firing rate and long-time average from simulation, with 5000 sets of parameters; altered parameter from left to right and top to bottom: recurrent connectivities S^{XY} , synaptic timescale τ^{XY} , synaptic coupling probabilities P^{XY} , refractory period τ_{ref}^X and external input rate $\lambda^{X,ext}$. **B:** absolute prediction error versus network synchrony, quantified by SSI.

guess for \bar{H}^{XY} , then updating ρ_∞^X , f^Y , and \bar{H}^{XY} recursively. This process effectively assumes that the synaptic drives H^{XY} evolve on a much faster timescale than ρ^X , allowing Eq. (5) to equilibrate quickly whenever ρ^X changes.

We test the Type I estimator on 5000 parameter sets, including variations in recurrent connectivities S^{XY} , synaptic coupling probabilities P^{XY} , external input rate $\lambda^{X,ext}$, synaptic timescale τ^{XY} , and refractory period τ_{ref}^X (Fig. 2; see Table I for tested parameter ranges). Our first finding is that the Type I estimator performs well when parameter variation mainly affects the equilibrium firing rates of the E and I populations, rather than the degree of synchrony. As shown in the three left panels of Fig. 2A, estimation errors are mostly within 10%, consistent with results from single-neuron simulations. Poor performance is observed only in two extreme cases: (1) when the SNN undergoes a sharp phase transition between silence and high firing activity (e.g., data points

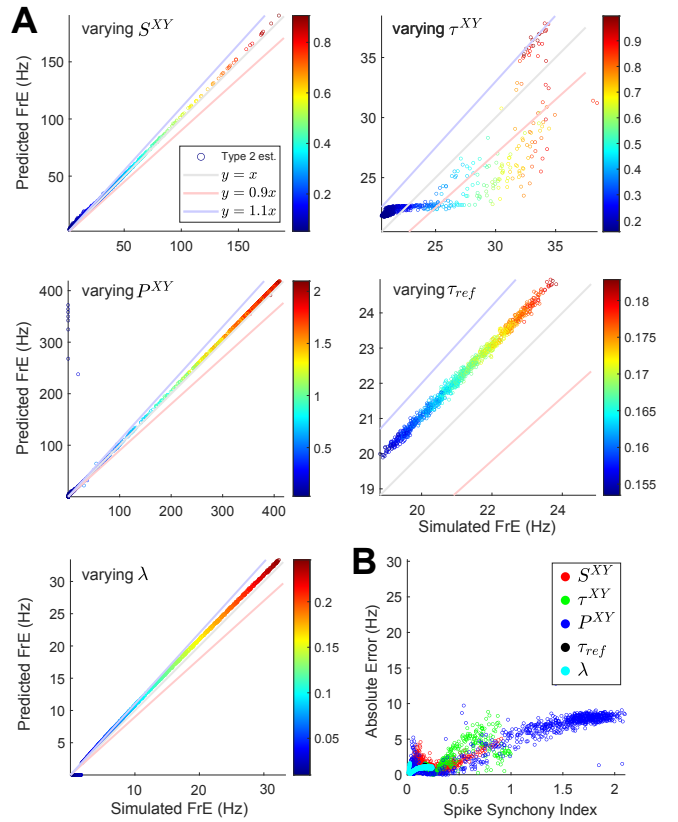


FIG. 3. Predictions of the full method versus ground truth from simulations. **A:** comparison of predicted steady-state firing rate and long-time average from simulation, tested on the same sets of parameters as in Fig. 2. **B:** absolute prediction error versus network synchrony, quantified by SSI.

along the y-axis in the P^{XY} panel; see Appendix for further analysis), and (2) when the firing rate is very low ($f^E < 5$ Hz), where spikes are very sensitive to small fluctuations (e.g., λ panel).

However, since the Type I estimator does not account for synchrony, it fails under changes in synaptic timescales (Fig. 2A, varying τ^{XY}), producing nearly identical predictions despite large variations in simulated firing rates. Notably, a higher degree of synchrony—measured by the spike synchrony index (SSI; see Appendix)—correlates with larger estimation error, as indicated by the warmer-colored data points. This failure arises because the Type I estimator neglects synaptic dynamics, which are known to play a crucial role in shaping network synchrony (see, e.g., [32, 38, 39]).

A similar issue arises when varying τ^X_{ref} (Fig. 2A). In highly synchronous states, most neurons fire and enter refractory periods simultaneously. As a result, they do not experience the peak of \bar{H}^{XY} , which follows the large instantaneous firing rate f_t^Y . This makes the simulated firing rate largely insensitive to τ^X_{ref} under high synchrony, as it is instead determined by how quickly synchronized neurons reach threshold after leaving the refractory state. In contrast, predictions based on Eq. (8)

Parameter	Definition	Typical Value	Tested Range
S^{EE}	E-to-E synaptic weight	5	4-6
S^{EI}	I-to-E synaptic weight	4.91	4-6
S^{IE}	E-to-I synaptic weight	2	1.5-2.5
S^{II}	I-to-I synaptic weight	4.91	4-6
P^{EE}	E-to-E coupling probability	0.15	0.05-0.45
P^{EI}	I-to-E coupling probability	0.5	0.05-0.85
P^{IE}	E-to-I coupling probability	0.5	0.05-0.85
P^{II}	I-to-I coupling probability	0.4	0.05-0.65
$\lambda^{E,\text{ext}}$	external-to-E input rate	7 kHz	0.1-10 kHz
$\lambda^{I,\text{ext}}$	external-to-I input rate	7 kHz	kept at the same value as λ^E
τ^{EE}	E-to-E synapse timescale	4 ms	1-5 ms
τ^{EI}	I-to-E synapse timescale	4.5 ms	4-5
τ^{IE}	E-to-I synapse timescale	1.2 ms	0.5-2 ms
τ^{II}	I-to-I synapse timescale	4.5 ms	4-5
τ_{ref}^E	E-refractory period	2 ms	0.8-2.3 ms
τ_{ref}^I	I-refractory period	1.6 ms	0.8-2.3 ms

TABLE I. Parameters tested. Typical values and tested ranges of parameters are provided.

show both a distorted ρ_∞^X and an inverted dependence of f^X on τ_{ref}^X .

Finally, we examine how prediction error correlates with synchrony (Fig. 2B). For most parameter sets, the absolute prediction error increases with SSI. A notable exception occurs when varying τ_{ref} (black dots), since in highly synchronized regimes, changing τ_{ref} has minimal effect on network behavior. Conversely, prediction errors are more sensitive to SSI when varying τ^{XY} (green dots). Extreme cases associated with phase transitions due to changes in P^{XY} were excluded from Fig. 2B to better highlight this relationship.

Type II estimator for spiking networks. We now test the Type II estimator on the same 5000 parameter sets used for Type I. Fig. 3 shows that by accounting for the dynamics of the first moment of synaptic activity, the Type II estimator more accurately recovers the average firing rate, even under changes in synaptic and refractory timescales (Fig. 3A, varying τ^{XY} and τ_{ref}). Specifically, for varying τ^{XY} , more than 84% of cases exhibit relative errors below 10%, and more than 92% fall below 30%. Across other parameters, Type II consistently outperforms Type I, as seen in the lower prediction errors presented in Fig. 3B.

Comparison with previous methods. Finally, we compare our estimators with two existing approximation methods: the mean-driven limit [36, 37] and the MF+v algorithm [35], as shown in Fig. 4. Our method outperforms both alternatives in the majority of parameter sets, achieving lower prediction errors and improved computational efficiency. This is clearly seen in Fig. 4B, where black dots (the Type II estimator) correspond to the smallest errors.

We conclude the results section with two additional observations on the differences between the three approaches. First, the mean-driven limit is analytically convenient, offering closed-form expressions for firing rates

(e.g., Eq.(4.11) in [36]). However, it does not consider synaptic or detailed neuronal dynamics. As a result, its predictions are completely insensitive to τ^{XY} (see blue dots in Fig. 4A), and the formulation cannot incorporate information about neuronal refractory periods. Moreover, its assumption of weak synaptic coupling leads to large prediction errors when varying S^{XY} .

In contrast, the MF+v method generates mean-field predictions by integrating detailed single-neuron dynamics obtained from simulations. While it does not account for synchrony either, it generally provides more accurate predictions than the mean-driven limit. However, because it still ignores collective dynamics, its applicability is limited in regimes where network synchrony plays a critical role. By directly modeling both neuronal and synaptic population dynamics, our estimators provide a more accurate and computationally efficient solution for firing rate prediction in finite-size SNNs.

V. DISCUSSION

This work provides a computationally efficient and simulation-free method for estimating firing rates in spiking neural networks (SNNs), offering broad applicability across theoretical and computational neuroscience. By formulating SNNs as Markov chains and carefully reducing their dimensionality, our approach captures essential network properties, including transient synchrony, without relying on the sweeping simplifications that typify many standard frameworks. In contrast, neural field models, Fokker-Planck equations, and kinetic theories commonly assume infinite network size, weak synaptic coupling, or complete input homogeneity [23, 40-43]. These assumptions facilitate analysis but often fail to reflect the rich and delicate dynamics observed in finite-sized, strongly connected neuronal circuits.

Algorithm	Type I	Type II	MF+v	Mean driven limit	Leaky IF (10 seconds)
Average runtime (s)	0.09	0.74	1.65	0.01	3.78

TABLE II. Comparison of average runtime for different algorithms. Tested on 600 sets of parameters and took the average; the leaky IF (integrate-and-fire) model was simulated for 10 seconds.

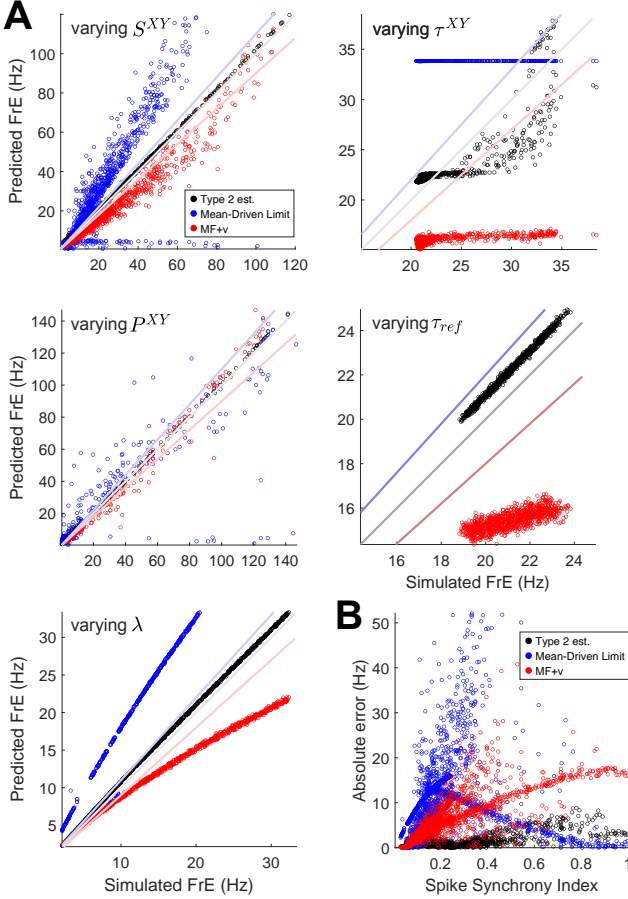


FIG. 4. Comparison of the Type II estimator, the mean-driven limit, and the MF+v algorithm. **A:** comparison in predicted firing rate with both methods, tested on 5000 sets of parameters, where the refractory period $\tau^{X,ref}$ is enforced to be 0 due to limitations of the mean driven limit; altered parameter from left to right and top to bottom: recurrent connectivities S^{XY} , synaptic timescale τ^{XY} , synaptic coupling probabilities P^{XY} , refractory period $\tau^{X,ref}$ and external input rate $\lambda^{X,ext}$. Note that the fourth subplot is not applicable to the method of mean-driven limit as explained above. **B:** comparison in absolute predictive error with both methods.

One of the key advantages of our Markovian formulation is its direct accommodation of firing, refractory, and resetting processes as discrete state transitions. This feature addresses a persistent obstacle in analyzing SNNs, namely the inherent discontinuity introduced when neurons spike and reset. Conventional mean-field approximations, for instance, often omit refractory periods or restrict coupling strengths and network sizes [36, 37].

While such approximations simplify the mathematics, they can obscure critical dynamical phenomena. Here, the Markov chain perspective retains biological fidelity by preserving these discontinuous events, allowing analytical studies of network behavior without sacrificing key mechanistic details.

Our results highlight a critical shortcoming of traditional first-order firing-rate estimators: when network synchronization or other higher-order correlations become significant, mean activity alone proves inadequate for accurate firing-rate predictions. By integrating the simplest form of higher-order dynamics—spike synchrony—we find that estimator accuracy improves markedly. This finding underscores the broader principle that higher-order correlations in nonlinear dynamical systems can decisively shape emergent behavior, even if they appear minimal from a low-dimensional perspective [44–47]. In doing so, our work also contributes to a larger body of research in complex systems, illustrating how interplay between coarse statistics and intricate interactions can guide the collective evolution of networked units. These insights provide a foundation for future explorations of high-dimensional neuronal circuits and open avenues for refining analytical methods that more comprehensively capture the nuanced behavior of biological networks.

Appendix A: Possible state transitions of single Markov neurons

1. for $m \neq \mathcal{R}$, one pending E -kick can cause the transitions $m \rightarrow \begin{cases} m + [S^{XE}] \\ m + [S^{XE}] + 1 \end{cases}$ with rates $\frac{\bar{H}^{XE}}{\tau^{XE}} \cdot \begin{cases} 1 - \{S^{XE}\} \\ \{S^{XE}\} \end{cases}$ or $m \rightarrow \mathcal{R}$ if the resulting state exceeds $m^{X,\text{th}}$;
2. similarly, for $m \neq \mathcal{R}$, one external kick can cause the transitions $m \rightarrow \begin{cases} m + [S^{X,\text{ext}}] \\ m + [S^{X,\text{ext}}] + 1 \end{cases}$ with rates $\lambda^{X,\text{ext}} \cdot \begin{cases} 1 - \{S^{X,\text{ext}}\} \\ \{S^{X,\text{ext}}\} \end{cases}$ or $m \rightarrow \mathcal{R}$ if the resulting state exceeds $m^{X,\text{th}}$;
3. for $m \neq \mathcal{R}$, one pending I -kick can decrease the membrane potential, leading to the state transitions $m \rightarrow \begin{cases} m - [\tilde{S}^{XI}(m)] \\ m - [\tilde{S}^{XI}(m)] - 1 \end{cases}$ with rates $\frac{\bar{H}^{XI}}{\tau^{XI}}$.

$$\begin{cases} 1 - \{\tilde{S}^{XI}(m)\} & \text{or } m \rightarrow -m^I \text{ if the resulting state is lower than } -m^I, \text{ where } \tilde{S}^{XI}(m) := \\ \{\tilde{S}^{XI}(m)\} & S^{XI} \cdot \frac{m+m^I}{m^{X,\text{th}}+m^I} > 0; \end{cases}$$

4. for $m \neq \mathcal{R}$, passive leakage brings the membrane potential one state closer to the reset potential 0, leading to the state transition $m \rightarrow m - \text{sgn}(m)$ with rate $\frac{m}{\tau_{\text{leak}}}$;
5. finally, for $m = \mathcal{R}$, the neuron can come out of the refractory state to the reset potential 0, leading to the state transition $m = \mathcal{R} \rightarrow 0$ with rate $\frac{1}{\tau_{X,\text{ref}}}$.

Appendix B: Instantaneous firing rates

The instantaneous firing rate f^X can be expressed by

$$\begin{aligned} f^X = & \frac{\bar{H}^{XE}}{\tau^{XE}} \sum_{m \geq m^{X,\text{th}} - [S^{XE}]} \rho_t^X(m) \\ & + \frac{\bar{H}^{XE}}{\tau^{XE}} \cdot \{S^{XE}\} \cdot \rho_t^X(m^{X,\text{th}} - [S^{XE}] - 1) \\ & + \lambda^{X,\text{ext}} \cdot \sum_{m \geq m^{X,\text{th}} - [S^{X,\text{ext}}]} \rho_t^X(m) \\ & + \lambda^{X,\text{ext}} \cdot \{S^{X,\text{ext}}\} \cdot \rho_t^X(m^{X,\text{th}} - [S^{X,\text{ext}}] - 1). \quad (\text{B1}) \end{aligned}$$

Appendix C: Type II estimator captures branching phenomena in LIF networks of different sizes

In certain parameter regimes, LIF networks experience a sharp phase transition between an inert state (E-firing rate is close to 0) to an active state (E-firing rate $\gg 1$) as the synaptic coupling probabilities change. In addition, we find that the bifurcation point moves as initial

conditions vary, leading to branching phenomena in some cases (Fig. 5 panels for varying P^{EI} , black line). The Type II estimator accurately captures such phenomena in terms of both the values of branching points and the qualitative behavior after the transition, while the Type I estimator only captures one branch of bifurcation (Fig. 5). This also explains the outstanding prediction error on the y-axis in the panel for varying P^{XY} in Fig. 2.

We argue that the reason for the Type II estimator to be better in such cases is that the phase transition depends on second- and higher-order interactions within the network, which the Type II estimator takes into consideration by construction. Let us take second-order interactions as an example. Consider a network at its steady state, with α^E (resp. α^I) the proportion of E- (resp. I-) neurons that can fire by receiving 1 E-spike. If an E-neuron fires an E-spike, then on average, the E-spike will induce $P^{EE}\alpha^E N^E$ E-spike, P^{EE} of which will in turn be received by the neuron itself, i.e. the eventual E-effect (up to second-order) of an E-spike unto itself is

$$\Delta_E^{(2)} = (P^{EE})^2 \alpha^E N^E S^{EE}.$$

Likewise, the eventual I-effect (up to second-order) of an E-spike unto itself is

$$\Delta_I^{(2)} = P^{IE} P^{EI} \alpha^I N^I \tilde{S}^{EI}.$$

In order for the E-population to fire continuously and consistently, i.e., $f^E > 0$, we must have

$$f^E(\Delta_E^{(2)} - \Delta_I^{(2)}) + \lambda^E S^{E,\text{ext}} > 0,$$

which imposes a condition for $(P^{EE})^2$ and $P^{IE} P^{EI}$ to satisfy. Dependencies on higher-order interactions can be derived similarly. Therefore, since the Type II estimator takes second-order interactions into account by including \bar{H}^{XY} , it is better at capturing phenomena relying on higher-order interactions, such as the branching phenomenon.

- [1] X.-J. Wang, Probabilistic decision making by slow reverberation in cortical circuits, *Neuron* **36**, 955 (2002).
- [2] E. M. Izhikevich and G. M. Edelman, Large-scale model of mammalian thalamocortical systems, *Proceedings of the national academy of sciences* **105**, 3593 (2008).
- [3] C. Eliasmith, T. C. Stewart, X. Choo, T. Bekolay, T. DeWolf, Y. Tang, and D. Rasmussen, A large-scale model of the functioning brain, *science* **338**, 1202 (2012).
- [4] T. C. Potjans and M. Diesmann, The cell-type specific cortical microcircuit: relating structure and activity in a full-scale spiking network model, *Cerebral cortex* **24**, 785 (2014).
- [5] H. Markram, E. Muller, S. Ramaswamy, M. W. Reimann, M. Abdellah, C. A. Sanchez, A. Ailamaki, L. Alonso-Nanclares, N. Antille, S. Arsever, *et al.*, Reconstruction and simulation of neocortical microcircuitry, *Cell* **163**, 456 (2015).
- [6] M. J. Bezaire, I. Raikov, K. Burk, D. Vyas, and I. Soltesz, Interneuronal mechanisms of hippocampal theta oscillations in a full-scale model of the rodent cal circuit, *Elife* **5**, e18566 (2016).
- [7] L. Chariker, R. Shapley, and L.-S. Young, Orientation selectivity from very sparse lgn inputs in a comprehensive model of macaque v1 cortex, *Journal of Neuroscience* **36**, 12368 (2016).
- [8] M. Schmidt, R. Bakker, K. Shen, G. Bezgin, M. Diesmann, and S. J. van Albada, A multi-scale layer-resolved spiking network model of resting-state dynamics in macaque visual cortical areas, *PLOS Computational Biology* **14**, e1006359 (2018).
- [9] Y. N. Billeh, B. Cai, S. L. Gratiy, K. Dai, R. Iyer, N. W. Gouwens, R. Abbasi-Asl, X. Jia, J. H. Siegle, S. R. Olsen,

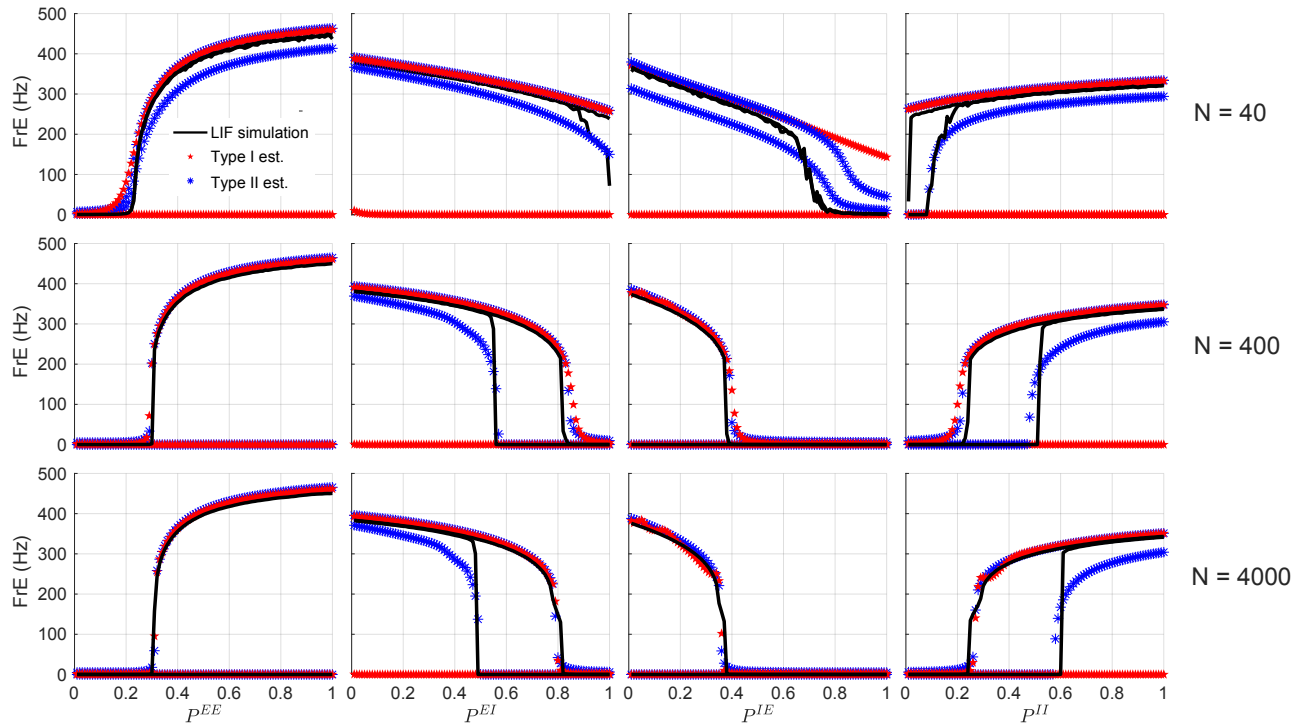


FIG. 5. Type II estimator captures the branching phenomena in LIF networks with different sizes. **Top row:** results in networks with 30 E-neurons and 10 I-neurons; **Middle row:** networks with 300 E-neurons and 100 I-neurons; **Bottom row:** networks with 3000 E-neurons and 1000 I-neurons. Each panel compares the steady-state firing rate predicted by Type-I and Type-II estimators and the long-time average (10 seconds) from simulation with different initial conditions for each set of parameters. Altered parameters are synaptic coupling probabilities P^{XY} . Different branches of LIF simulations and estimators come from different initial conditions.

et al., Systematic integration of structural and functional data into multi-scale models of mouse primary visual cortex, *Neuron* **106**, 388 (2020).

- [10] J. H. Siegle, X. Jia, S. Durand, S. Gale, C. Bennett, N. Graddis, G. Heller, T. K. Ramirez, H. Choi, J. A. Luviniano, *et al.*, Survey of spiking in the mouse visual system reveals functional hierarchy, *Nature* **592**, 86 (2021).
- [11] F. Zenke and T. P. Vogels, The remarkable robustness of surrogate gradient learning for instilling complex function in spiking neural networks, *Neural computation* **33**, 899 (2021).
- [12] L. Chariker, R. Shapley, M. Hawken, and L.-S. Young, A computational model of direction selectivity in macaque v1 cortex based on dynamic differences between on and off pathways, *Journal of Neuroscience* **42**, 3365 (2022).
- [13] M. M. Woodman and V. K. Jirsa, Emergent dynamics from spiking neuron networks through symmetry breaking of connectivity, *PLoS One* **8** (2013).
- [14] E. M. Izhikevich, Which model to use for cortical spiking neurons?, *IEEE transactions on neural networks* **15**, 1063 (2004).
- [15] F. Zenke, E. J. Agnes, and W. Gerstner, Diverse synaptic plasticity mechanisms orchestrated to form and retrieve memories in spiking neural networks, *Nature communications* **6**, 6922 (2015).
- [16] R. Gast, T. R. Knösche, and H. Schmidt, Mean-field approximations of networks of spiking neurons with short-term synaptic plasticity, *Physical Review E* **104** (2021).
- [17] F. J. Schmitt, V. Rostami, and M. P. Nawrot, Efficient parameter calibration and real-time simulation of large-scale spiking neural networks with genn and nest, *Frontiers in Neuroinformatics* **17** (2023).
- [18] M. Stimberg, D. F. M. Goodman, and T. Nowotny, Brian2genn: accelerating spiking neural network simulations with graphics hardware, *Scientific Reports* **10** (2020).
- [19] S. R. Kulkani, M. Parsa, J. P. Mitchell, and C. D. Schuman, Benchmarking the performance of neuromorphic and spiking neural network simulators, *Neurocomputing* **447**, 145 (2021).
- [20] K. Mizuseki and G. Buzsáki, Preconfigured, skewed distribution of firing rates in the hippocampus and entorhinal cortex, *Cell Reports* **4**, 1010 (2013).
- [21] R. E. Kass, H. Bong, M. Olarinre, Q. Xin, and K. N. Urban, Identification of interacting neural populations: methods and statistical considerations, *Journal of Neurophysiology* (2023).
- [22] P. Dayan and L. F. Abbott, *Theoretical neuroscience*, The MIT Press, ISBN: 9780262041997 (2001).
- [23] H. R. Wilson and J. D. Cowan, Excitatory and inhibitory interactions in localized populations of model neurons, *Biophysical journal* **12**, 1 (1972).
- [24] A. V. Rangan and D. Cai, Maximum-entropy closures for kinetic theories of neuronal network dynamics, *Phys. Rev. Lett.* **96**, 178101 (2006).
- [25] M. A. Buice and C. C. Chow, Dynamic finite size effects

in spiking neural networks, PLoS computational biology **9**, e1002872 (2013).

[26] J. F. Ramirez-Villegas, K. F. Willeke, N. K. Logothetis, and M. Besserve, Dissecting the synapse-and frequency-dependent network mechanisms of *in vivo* hippocampal sharp wave-ripples, *Neuron* **100**, 1224 (2018).

[27] W. Gerstner, W. M. Kistler, R. Naud, and L. Paninski, *Neuronal dynamics: From single neurons to networks and models of cognition* (Cambridge University Press, 2014).

[28] C. Koch, *Biophysics of computations* (1999).

[29] D. McLaughlin, R. Shapley, M. Shelley, and D. J. Wielaard, A neuronal network model of macaque primary visual cortex (v1): Orientation selectivity and dynamics in the input layer 4ca, *Proceedings of the National Academy of Sciences* **97**, 8087 (2000).

[30] H. Dale, *Pharmacology and nerve-endings* (1935).

[31] E. R. Kandel, J. H. Schwartz, T. M. Jessell, S. Siegelbaum, A. J. Hudspeth, S. Mack, *et al.*, *Principles of neural science*, Vol. 4 (McGraw-hill New York, 2000).

[32] J. Chang, Z. Li, Z. Wang, L. Tao, and Z. Xiao, Minimizing information loss reduces spiking neuronal networks to differential equations, *arXiv preprint*, arXiv:2411.14801 (to appear in *Journal of Computational Physics*) (2025).

[33] Y. Li and H. Xu, Stochastic neural field model: multiple firing events and correlations, *Journal of mathematical biology* **79**, 1169 (2019).

[34] Y. Li, L. Chariker, and L.-S. Young, How well do reduced models capture the dynamics in models of interacting neurons?, *Journal of mathematical biology* **78**, 83 (2019).

[35] Z.-C. Xiao, K. K. Lin, and L.-S. Young, A data-informed mean-field approach to mapping of cortical parameter landscapes, *PLoS Computational Biology* **17**, e1009718 (2021).

[36] D. Cai, L. Tao, A. V. Rangan, D. W. McLaughlin, *et al.*, Kinetic theory for neuronal network dynamics, *Communications in Mathematical Sciences* **4**, 97 (2006).

[37] A. Treves, Mean-field analysis of neuronal spike dynamics, *Network* **4**, 259 (1993).

[38] X.-J. Wang and G. Buzsáki, Gamma oscillation by synaptic inhibition in a hippocampal interneuronal network model, *Journal of Neuroscience* **16**, 6402 (1996).

[39] S. Keeley, Á. Byrne, A. Fenton, and J. Rinzel, Firing rate models for gamma oscillations, *Journal of Neurophysiology* **121**, 2181 (2019).

[40] N. Brunel, Dynamics of sparsely connected networks of excitatory and inhibitory spiking neurons, *Journal of computational neuroscience* **8**, 183 (2000).

[41] N. Brunel and V. Hakim, Fast global oscillations in networks of integrate-and-fire neurons with low firing rates, *Neural computation* **11**, 1621 (1999).

[42] D. Nykamp and D. Tranchina, A population density approach that facilitates large-scale modeling of neural networks: Analysis and an application to orientation tuning, *J. Comput. Neurosci.* **8**, 19 (2000).

[43] F. Baccelli and T. Taillefumier, The pair-replica-mean-field limit for intensity-based neural networks, *SIAM Journal on Applied Dynamical Systems* **20** (2021).

[44] E. Schneidman, M. J. I. Berry, R. Segev, and W. Bialek, Weak pairwise correlations imply strongly correlated network states in a neural population, *Nature* (2006).

[45] N. A. Cayco-Gajic, J. Zylberberg, and E. Shea-Brown, Triplet correlations among similarly tuned cells impact population coding, *Frontiers in Computational Neuroscience* (2015).

[46] F. Montani, A. Kohn, M. A. Smith, and S. R. Schultz, The role of correlations in direction and contrast coding in the primary visual cortex, *J Neurosci* (2007).

[47] S. Nirenberg and P. E. Latham, Decoding neuronal spike trains: how important are correlations?, *Proc Natl Acad Sci U S A* (2003).